2021

Application of Computational Fluid Dynamics to the Lubrication Study of an Oil-injected Screw Compressor

Sheng-Hung Hsieh
Hanbell Precise Machinery Co. Ltd., Taiwan, shhsieh@hanbell.com

Jin-Wei Zhang

Chi-Shun Huang

Application of Computational Fluid Dynamics to the Lubrication Study of an Oil-injected Screw Compressor

Sheng-Hung Hsieh*, Jin-Wei Zhang, Chi-Shun Huang

Hanbell Precise Machinery Co. Ltd., Taiwan
Taoyuan City, Taiwan (R.O.C.)

* shhsieh@hanbell.com

ABSTRACT

Computational fluid dynamics and mesh generation tools have been well developed, and could be used to calculate the performance of an oil-injected screw compressor. Designers could now effectively obtain reliable results of efficiency, temperature, force and torque. Some physical phenomena inside a screw compressor are not easy to be observed through experiments, such as the oil distribution and the oil film thickness on the rotor surface. Under the ideal lubrication condition, the oil film of proper thickness should be maintained on the local surfaces which are going to contact with each other. This could be numerically explored by computational fluid dynamics. The first case in this study showed the effect of centrifugal force on a thin free surface flow on the rotor surface. Designers could graphically understand how the oil film flows on the rotor surface when rotors separately rotate without meshing with each other and doing the compression work. The second case in this study was the rotor lubrication. The clearance distribution between rotors in the actual contact area was designed by the minimum film thickness and was 1 μm. The pressure gradient on the rotor surface was used to see if the hydrodynamic pressure appeared. Designers could optimize the design of oil injection not only by considering efficiencies, but also by analyzing the pressure gradient and the oil film distribution on rotor surfaces.

1. INTRODUCTION

The gas is compressed by a pair of rotors in an oil-injected screw compressor. During the compression process, the proper quantity of oil is injected into the compressor to reduce the leakage flow rate, and to cool the compressed gas temperature. The rotors are also lubricated by the oil for the long-time operation. The designer could effectively predict the performance of a screw compressor by using the well-developed thermodynamic model and computational fluid dynamics (CFD) tools. The pressure curve, efficiencies, the gas power consumption, the gas force, and the gas torque could be accurately and efficiently calculated. However, there were few recent studies that focused on the rotor lubrication in the screw compressor. In the previous studies of the bearing lubrication, there were rich references to the theoretical model and the experimental verification.

The rotors in the screw compressor could be considered as two cylinders which were in rotational contact with each other. Hydrodynamic lubrication or Elastohydrodynamic lubrication (EHD or EHL) would appear in the contact area. The pressure of oil rises rapidly. The pressure gradient in the direction of rotation on the cylinder surface would be significant positive followed by negative (Zhang *et al*., 2019). The pressure distribution in the contact area would match the elastic Hertzian contact pressure distribution (Khonsari and Booser, 2008). Under the condition of flooded EHD, Dowson (1970) gave the equations to estimate the minimum film thickness. When the insufficient quantity of oil was in the contact area, the starved EHD appeared. Kostal *et al*. (2015, 2017) established the equipment to accurately measure the meniscus position and the oil film thickness. They experimentally examined the parameters in the equation of film thickness reduction. The parameters were presented by the study of point contact lubrication (Chevalier et al., 1998), and the study of elliptical contact lubrication (Damiens et al., 2004). Compared with the meniscus position as the criterion for determining the starvation level, the film thickness in the inlet area could be applied to identify the starvation level more clearly in the severely starved case, which film thickness reduction was less than 0.5 and the meniscus position was very close to the Hertzian contact circle. Kostal *et al*. (2017) presented

that the inlet film thickness was close to the central film thickness under severely starved lubrication. When the starvation level was improved, the film thickness reduction curves of different contact types would grow divergently. In the studies of the effect of centrifugal force on the liquid movement, Zamfirescu et al. (2004) numerically analyzed the liquid drop in the compression chamber. The liquid drop was affected by the centrifugal force and the gas flow, and filed away from the rotor center to stay on the housing and rotors' tips. Zoelen et al. (2008) studied the grease film on raceways of the taper roller bearing and the spherical roller bearing by experimental measurement and numerical analysis. Under the influence of centrifugal force, the transient film thickness distribution curves on these two raceways were different. These studies showed that the surface film thickness was a key parameter of the rotor lubrication. In order to achieve the good lubrication on rotors which were in rotational contact with each other, the oil might first fly to the rotor surface and then formed an oil film. The oil film driven by the centrifugal force, the air flow velocity, and the pressure difference would flow on the rotor surface. The oil film of proper thickness should be maintained on the local surfaces which were going to contact with each other. Finally, the hydrodynamic lubrication or EHD would appear in the contact area.

The goal of this study was to apply CFD to the lubrication study of an oil-injected screw compressor. In the grid model, the minimum film thickness calculated by the equation provided by Dowson (1970) was used to be the clearance between rotors in the actual contact area. TwinMesh was used to generate the dynamic grid model of the compression chamber. The built-in multi-phase flow model and free surface model in ANSYS CFX were used to calculate the oil distribution on rotor surfaces. Two cases were presented in this study. In the first case, rotors rotated separately. The transient oil distributions on rotor surfaces under the influence of centrifugal force were analyzed. In the second case, the six CFD models with different positions of oil injection ports were analyzed. The time-average axial distribution curves of the average volume fraction of oil on rotor surfaces were presented. The pressure gradient on rotor surface was used to see if the hydrodynamic pressure appeared, and would be one of the design objectives of the oil injection.

2. CFD MODEL AND GRID MODEL

The CFD model used in this study was based on an oil-injected screw compressor, which displacement is 260 m^3/hr at 3,000 rpm. Figure 1 (a) shows the solid model of the compressor which is constructed by the inlet part, a pair of "5x6" rotors, the outlet part, and the oil port(s). In order to reduce the physical calculation time, the simplified model of the compressor was adapted, as shown in Figure 1 (b). The continuous equations, momentum equations, and energy equations for the turbulence flow were solved by ANSYS CFX. The built-in inhomogeneous model and free surface model in ANSYS CFX were used to describe the multi-phase flow, and to present the oil distribution on rotor surfaces. The selected models and schemes in ANSYS CFX are listed in Table 1 (Rane *et al.*, 2016 and Basha *et al.*, 2018). The flow paths were divided into the dynamic and the static grid models. The dynamic grid model of compression chambers is shown in Figure 2 (a), and was generated by TwinMesh. The edge size of elements on the casing was about 2 mm. The edge size of elements on the interface between rotors was about 1 mm. The radial element number was 6. The first radial element height close to the rotor surface was about 0.1 mm. The axial element size was about 2 mm. There were about 310,000 elements in the dynamic grid model. The static grid models of the inlet part, the outlet part, and the oil port(s) are shown in Figure 2 (b). There were about 130,000 elements in the static grid models.

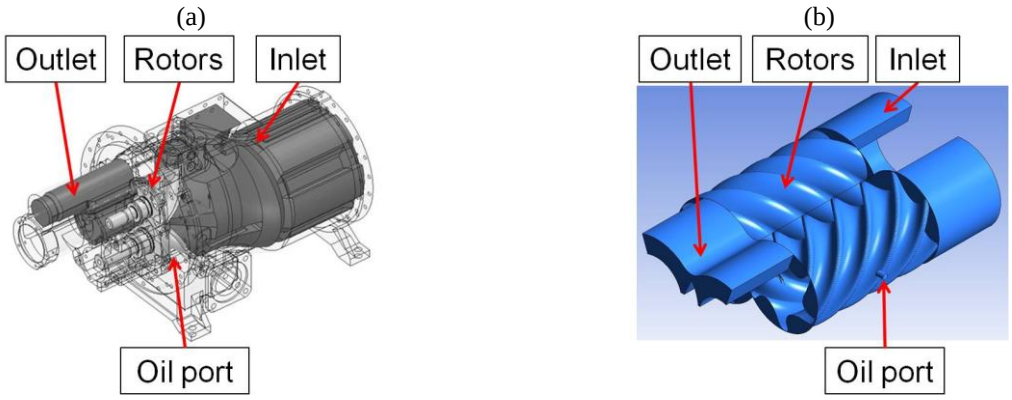

Figure 1: (a) The solid model, and (b) the simplified model of the oil-injected screw compressor

Table 1. The selected models and schemes in ANSYS CFX

Models and Schemes	Selection
Turbulence Model	SST
Multiphase Model	Inhomogeneous Model Free Surface Model
Advection Scheme	High Resolution
Turbulence Scheme	First Order Upwind
Transient Scheme	Second Order Backward Euler
Convergence Criterion	10^{-3} Max Residual Level

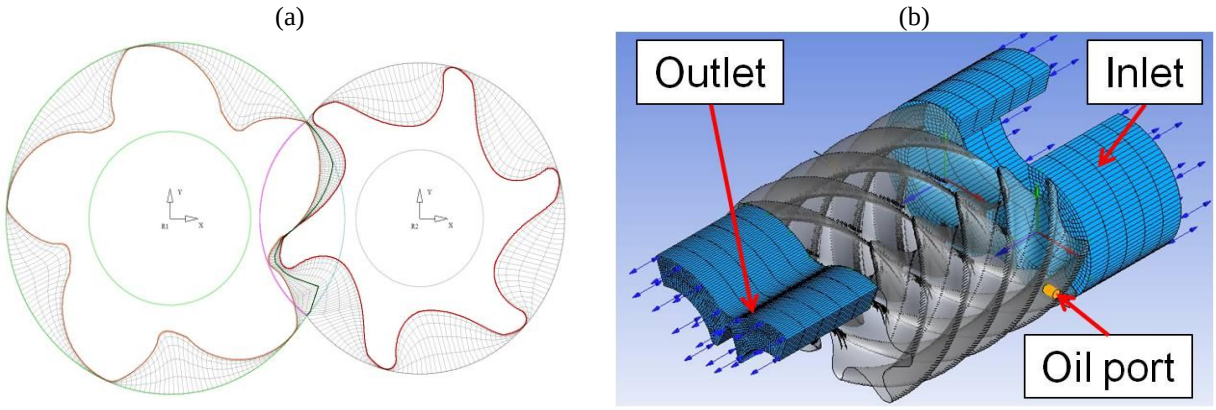

Figure 2: (a) The dynamic grid model, and (b) the static grid models of flow paths

The non-contact rotor profiles were needed to generate the dynamic grid model. Figure 3 (a) shows the concept design of clearance distribution between rotors. The proper clearance distribution should be designed on the rotor profiles to ensure that rotors rotated smoothly. The clearance was 0 μm on the parts of rotor profiles which were in contact with each other, and was 16 μm on the parts of rotor profiles which were not in contact with each other. When the rotors were lubricated by the oil, there was a thin oil film in the actual contact area. The minimum oil film thickness could be calculated by Equation (1) (Dowson, 1970). The material parameter, the speed parameter, and the load parameter in Equation (1) were all listed in Table 2 and 3. The minimum oil film thickness was affected by the relative speed between rotors, material properties of oil and rotors, curvatures of surfaces, and the condition of load. In this study, the actual contact area was design on the profiles where the relative velocities between rotors were between 3 and 5 m/s. The clearance between rotors in the actual contact area was 1 μm. This ideal design of clearance distribution between rotors is shown in Figure 3 (b). In addition, the dynamic viscosity would be changed rapidly by pressure, and was given in Equation (2).

$$h_o/R = 2.65G^{0.54}U^{0.7}/W^{0.13} \tag{1}$$

$$G = \alpha E'$$

$$U = (\mu_0 u)/(E'R)$$

$$W = w/(E'LR)$$

$$\mu = \mu_o \exp(\alpha \cdot P) \tag{2}$$

μ_o : the dynamic viscosity at atmospheric (essentially zero) pressure

α : the pressure-viscosity coefficient

(a) (b)

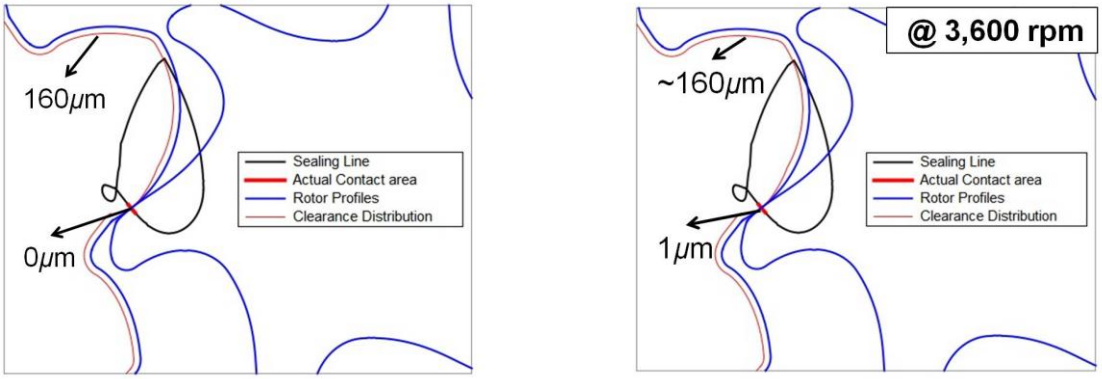

Figure 3: (a) The concept design, and (b) the ideal design of clearance distributions between rotors

Table 2. Material properties of fluids

Material Properties	**Unit**	**Value**
Primary fluid	--	R134a (ideal gas)
Secondary fluid	--	Oil
Density of oil	g/cc	0.92
Dynamic viscosity of oil (μ_o)	cP	36.13
Surface tension of oil	N/m	0.03
Contact angle of oil	--	45^o
Roelands' pressure-viscosity index (Z)	--	0.63
Pressure-viscosity coefficient (α)	Gpa^{-1}	0.02

Table 3. The minimum film thickness and the contact area width

Parameter	**Unit**	**Value @ 3,600 rpm**		
Relative speed	m/s	1~3	3~5	5~7
Minimum Film Thickness(h_o)	mm	0.0006	0.0010	0.0015
Contact area width ($2b$)	mm	0.138	0.138	0.151
Max. Hertzian contact pressure (P_o)	MPa	241.2	226.5	212.1
h_o/R	$x10^5$	3.869	6.118	7.448
Material Parameter (G)		4,454.2	4,454.2	4,454.2
Pressure-viscosity coefficient (α)	Gpa^{-1}	0.020	0.020	0.020
Young's modulus (E)	N/mm^2	202,000	202,000	202,000
Poisson's ratio (γ)		0.280	0.280	0.280
E'	N/mm^2	219,184	219,184	219,184
Speed Parameter (U)	$x10^{11}$	2.121	3.988	5.154
Dynamic viscosity (μ_o)	cP	36.13	36.13	36.13
u	mm/s	2,024.0	4,047.1	6,095.6
R_1	mm	30.3	30.3	30.3
R_2	mm	32.7	37.4	54.8
R	mm	15.7	16.7	19.5
Load Parameter (W)	$x10^6$	7.609	6.712	5.883
w	N	426.8	440.5	455.8
L	mm	16.3	17.9	18.1

3. RESULT AND DISCUSSION

There were two cases discussed in this section. In the first case, rotors rotated separately. The transient distribution of the volume fraction of oil on the rotor surface under the influence of the centrifugal force was analyzed. In the second case, six CFD models with different oil injection positions were analyzed by considering the CFD model and grid models presented in Section 2. The time-average axial distribution curves of the average volume fraction of oil on rotor surfaces were presented. The pressure gradient on the rotor surface was used to see if the hydrodynamic pressure appeared. The detailed calculation conditions and results of these two cases were explained and discussed in following sub-sections.

3.1 Effect of Centrifugal Force on Oil Film Flow on Rotor Surfaces

In this case, there was the thin film of uniform thickness on the rotor surface before the rotor rotation. Figure 4 shows the oil film domain and the gas domain in the CFD model. The oil film domain was full of oil to be the 50 µm thick thin film as the initial condition. The rotational wall (A) described the rotor surface in the CFD model. The opening type boundary condition (B) described the other surfaces in the CFD model. The rotational speed of the male rotor was 3,600 rpm, and the one of the female rotor was 3,000 rpm. Figure 5 shows the transient distribution of the volume fraction of oil on rotor surfaces when rotors have separately rotated 0, 1/8, 1/4, 1/2, and 1 turn. The oil film moved on the rotor surface toward the tip of rotor and left the rotor surface. Figure 6 shows the axial distribution curves of the average volume fraction of oil on rotor surfaces. These axial distribution curves were considered to be flat, and decreased significantly near the outlet end of the male rotor and the inlet end of the female rotor. Although the rotational speed of the male rotor was faster than the one of the female rotor, the average value of the distribution curve on the male rotor decreased a little slower than the one on the female rotor.

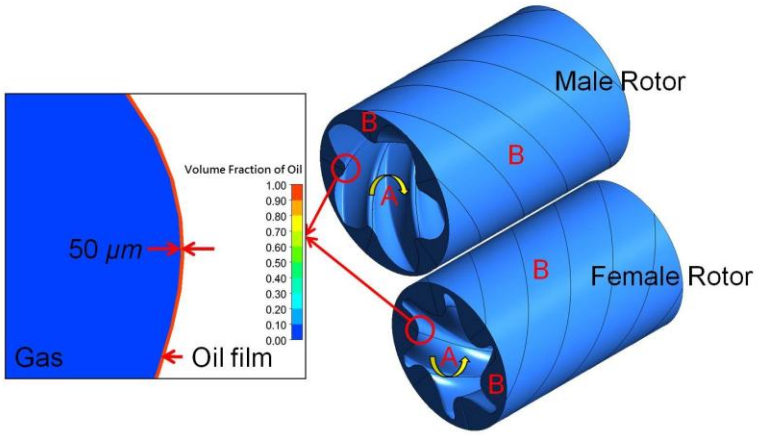

Figure 4: The initial condition and boundary conditions are used in the analysis of the effect of centrifugal force on oil film flow on rotor surfaces. "A" is the rotational wall. "B" is the opening type boundary condition.

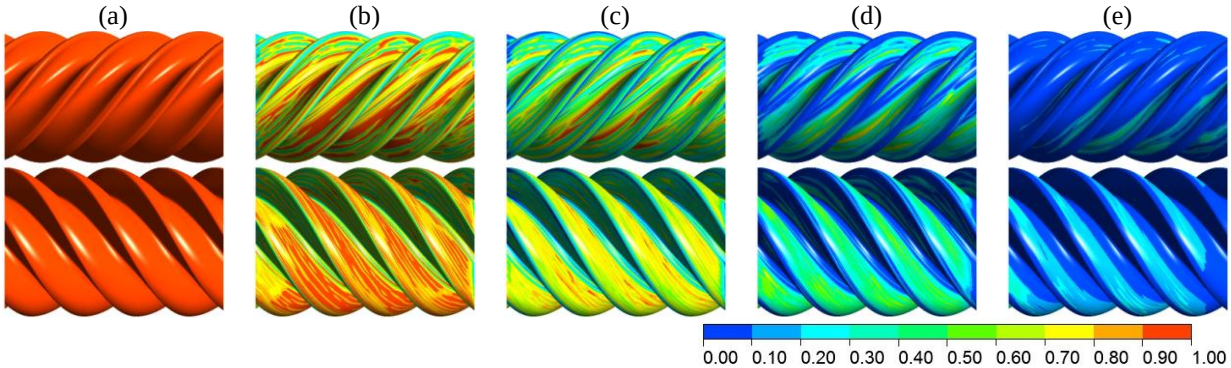

Figure 5: These contour graphs show the transient distributions of the volume fraction of oil on rotor surfaces when rotors have separately rotated (a) 0 turn, (b) 1/8 turns, (c) 1/4 turns, (d) 1/2 turns and (e) 1 turn.

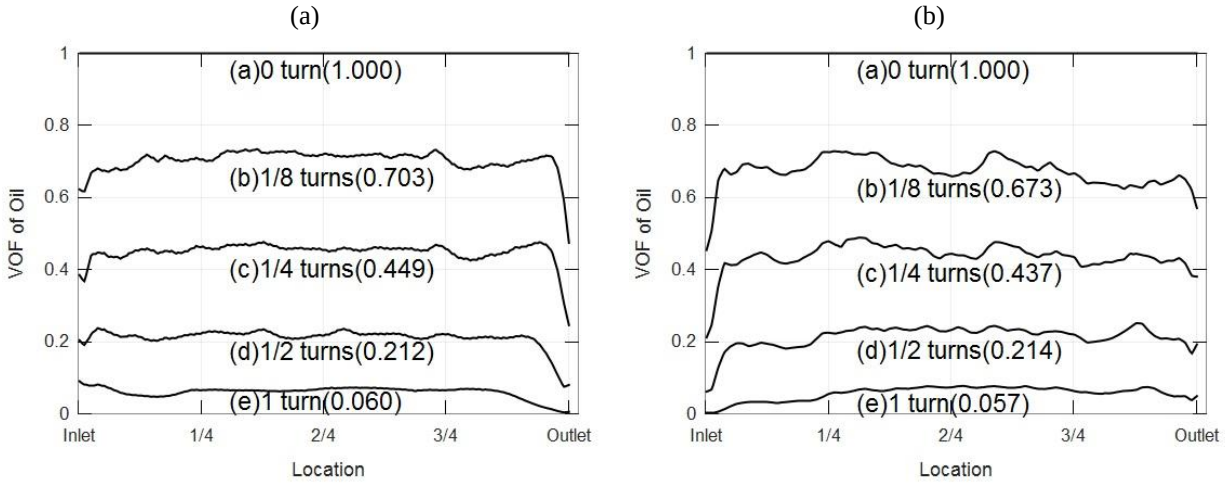

Figure 6: The axial distribution curves of the average volume fraction of oil on (a) the male rotor surface and (b) the female rotor surface

Figure 7 shows the distribution curves of the volume fraction of oil on tooth profiles in the middle of rotors. The wavy curves occurred when rotors rotated. Figure 7 (a) shows the distribution curves on the tooth profile in the middle of the male rotor. The average absolute radius gradient along the short side of the male rotor profile was 0.71, and the one along the long side of the male rotor profile was 0.41. The amplitude of the wavy curve on the short side was larger than the one on the long side. The values of distribution curves on the short side decreased faster than the ones on the long side. Figure 7 (b) shows the distribution curves on the tooth profile in the middle of the female rotor. The average absolute radius gradient along the short side of the female rotor profile was 0.76 mm, and the one along the long side of the female rotor profile was 0.55 mm. The amplitudes of the wavy curve on both sides of the female rotor profile were quite the same. The values of distribution curves on the short side decreased a little faster than the ones on the long side. When rotors have rotated one turn, the values of distribution curves on tooth flanks of both rotors were higher than the ones on roots and tips of both rotors.

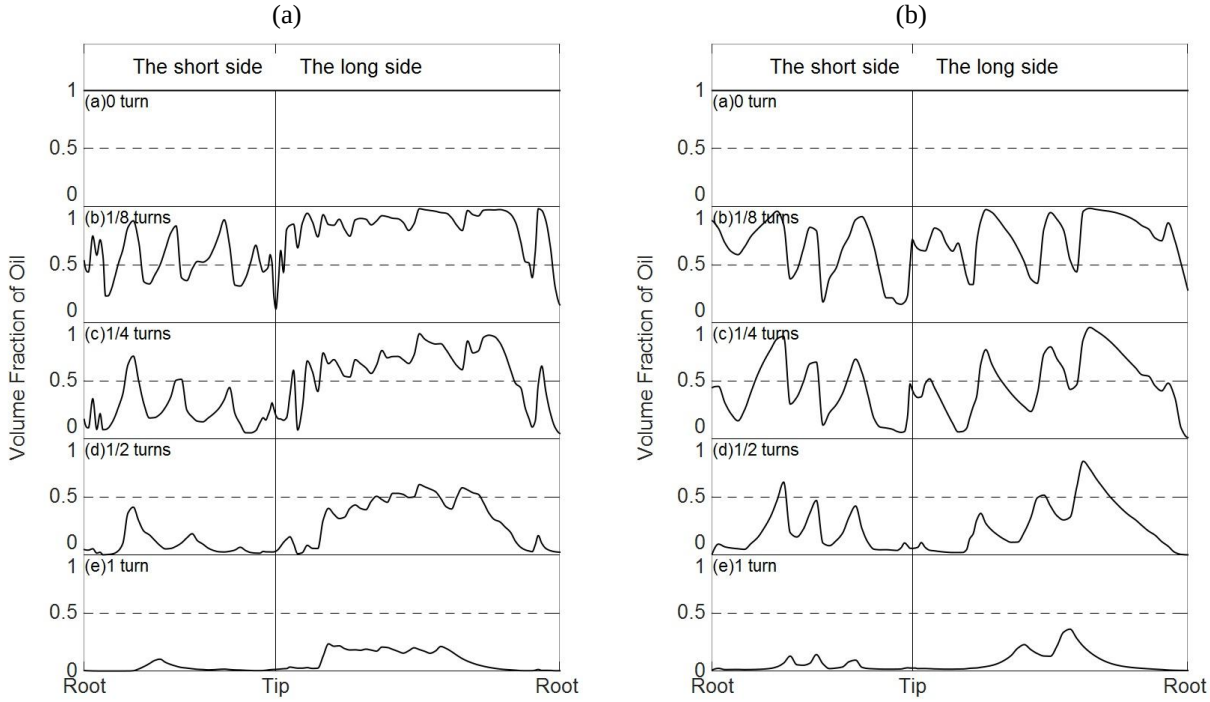

Figure 7: The distribution curves of the volume fraction of oil on tooth profiles in the middle of (a) the male rotor and (b) the female rotor

3.2 Oil Film Distribution and Pressure Gradient on Rotor Surfaces

In this case, the different oil injection ports were considered in six CFD models. The inlet pressure was 3.6 bar. The outlet pressure was 9.5 bar. The inlet temperature was 15 °C. The outlet temperature was 65 °C. Figure 8 (a) shows the positions of oil injection ports and six CFD models. The injection ports named M1 and F1 were located on the 1/4 length of rotor from the inlet end. The injection ports named M2 and F2 were located on the middle of rotors. The injection ports named M3 and F3 were located on the 1/4 length of rotor from the outlet end. The names of CFD models meant the oil was only injected through the corresponded named port(s). The oil flow rate of each injection port was 20 Litre/min. Figure 9 shows the contour graphs of the volume fraction of oil on rotor surfaces. After the oil was injected into the compression chamber, it would be collided with rotor surfaces. The oil would spread on surfaces of both rotors and be transported toward the outlet end. The oil on surfaces of both rotors would be transferred to each other in the meshing area. The oil distribution also changed for the centrifugal force, the gas flow, and the gas pressure difference. In the CFD model named M2, the oil was injected through the port named M2 on the side of the male rotor. Part of oil flowed to and was transferred to the female rotor surface. In the CFD model named F2, the oil was injected through the port named F2 on the side of the female rotor. Less of oil flowed to and was transferred to the male rotor surface.

The time-average axial distribution curves of the average volume fraction of oil on the entire rotor surface are shown in Figure 10 (a), and the ones on the local surface in the rotor meshing area are shown in Figure 10 (b). The rotor meshing area was between the cusps of the casing, where were 56° and 123° in the angle coordinate system shown in Figure 8 (b). Figure 10 shows that low values of distribution curves were between the oil injection port and the inlet end. All peak values of distribution curves appeared near the positions of oil injection ports. There was more oil collided with the male rotor surface than with the female rotor surface. Between the oil injection port and the outlet end, the distribution curves gradually dropped from peak points to become flat curves. Figure 10 (b) shows that there were noticeable distribution curves of the CFD model named M1F1. The positions of oil injection ports in this CFD model were closer to the inlet end than the ones in the other CFD models. The oil was widely distributed on the local surface in the rotor meshing area.

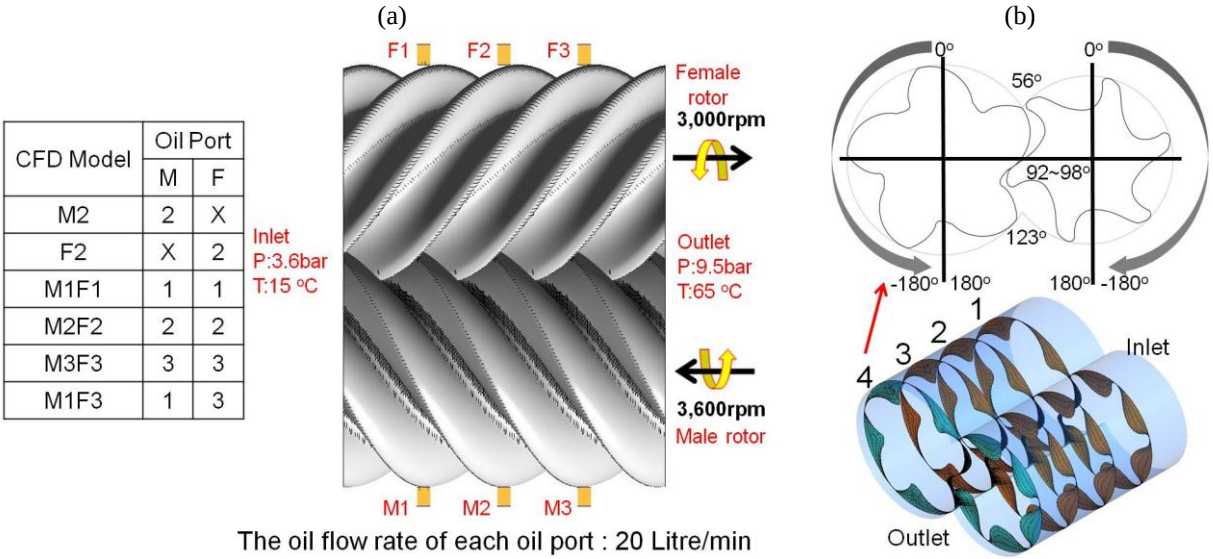

CFD Model	Oil Port	
	M	F
M2	2	X
F2	X	2
M1F1	1	1
M2F2	2	2
M3F3	3	3
M1F3	1	3

Figure 8: (a) Positions of oil injection ports and six CFD models, and (b) positions of four cross sections and the angular coordinate system

The pressure gradient along the rotor profile in the rotation direction on the rotor surface could be analyzed to understand if a good lubrication condition was in the actual contact area between rotors. Figure 11 shows the pressure gradient curves on male rotor surfaces of six CFD models at the same calculation time steps. These curves were obtained on four cross sections where rotors were actually in rotational contact with each other. The positions of these four cross sections and the angular coordinate system are shown in Figure 8 (b). The cross section 1 was near the oil injection ports named M1 and F1. There were the same correspondences for the cross sections 2 and 3 to the oil injection ports. The cross section 4 was near the outlet end. The actual contact area was between 92° and 98°.

The minimum clearance between rotors on these four cross sections all appeared at 96.21°. The values of pressure gradient curves shown in Figure 11 slightly changed between 84° and 94°. Peak values of most of pressure gradient curves appeared between 94° and 96°. The pressure would grow to the peak value when the pressure gradient curve drops from the peak to the zero. Most of these zero points of pressure gradient curves shown in Figure 11 appeared near 96°. However, the peak values of pressure did not match the Hertzian pressure. These curves only showed the phenomenon of hydrodynamic lubrication. Phenomenon of EHD did not appear in the actual contact area. One of the possible reasons was that the proper quantity of oil was not maintained in the actual contact area. Another one was that the edge size of element was larger than the actual contact area in the grid model. The spatial resolution was not good enough to show the pressure variation of EHD. Peak values of pressure gradient curves recorded in Figure 11 could be used to identify if the hydrodynamic pressure appeared near the actual contact area. In CFD models named M2, F2, M2F2 and M3F3, there were no obvious hydrodynamic pressure appeared on the cross section 1s. In CFD models named M1F1 and M1F3, the obvious hydrodynamic pressures appeared on four cross sections. The above analysis showed that the designer could check if the proper quantity of oil was maintained in the actual contact area based on the physical phenomenon of lubrication.

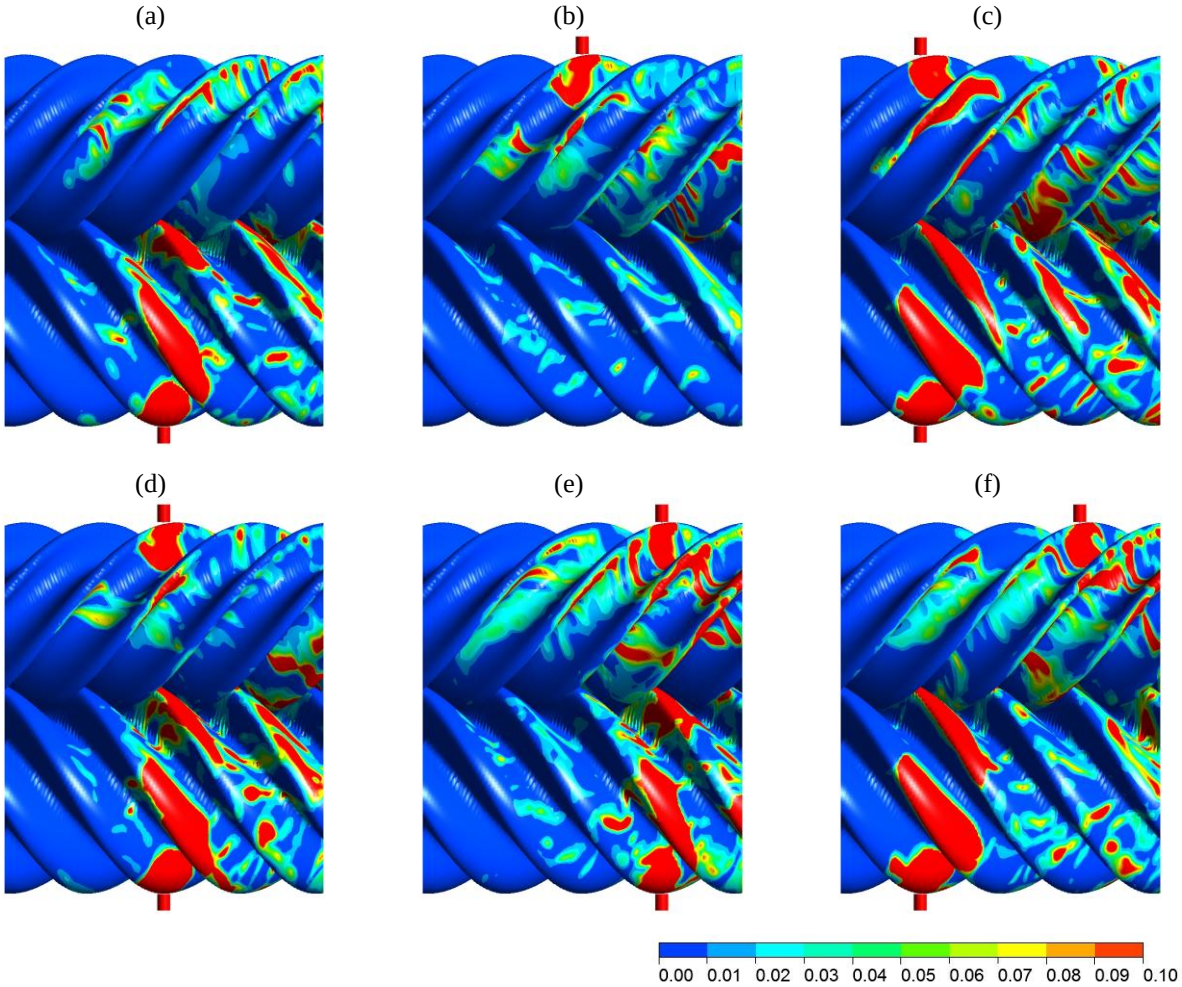

Figure 9: The contour graphs show the distributions of volume fraction of oil on rotor surfaces of CFD models named (a) M2, (b) F2, (c) M1F1, (d) M2F2, (e) M3F3, and (f) M1F3.

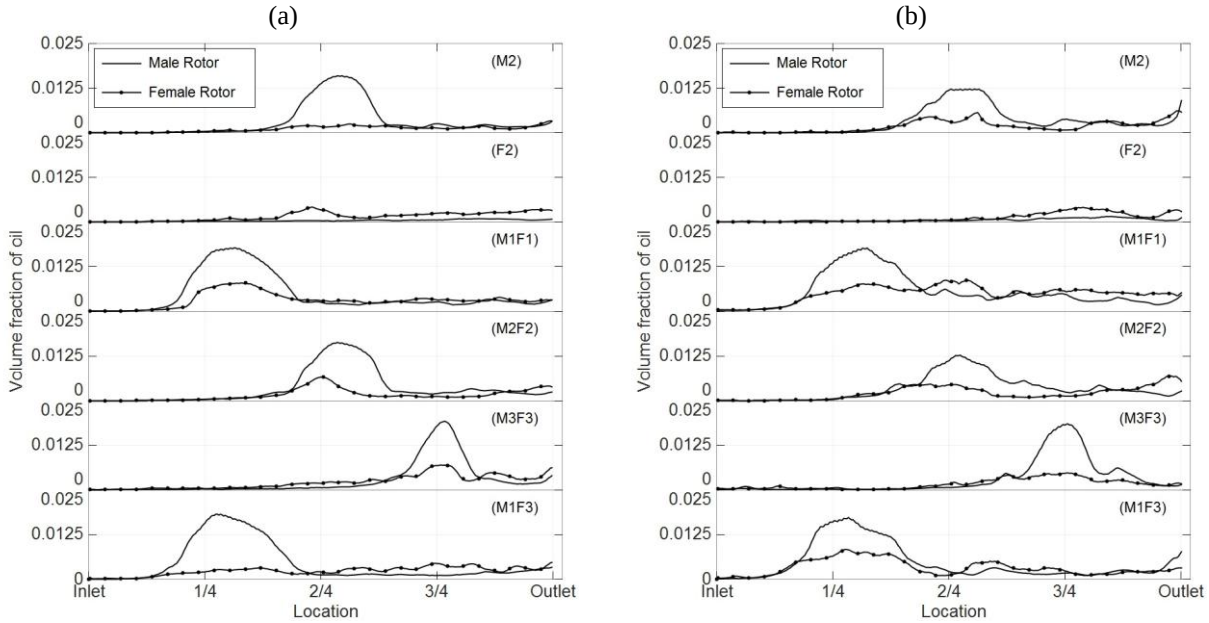

Figure 10: The time-average axial distribution curves of the average volume fraction of oil on (a) the entire rotor surface, and (b) the local surface in the rotor meshing area

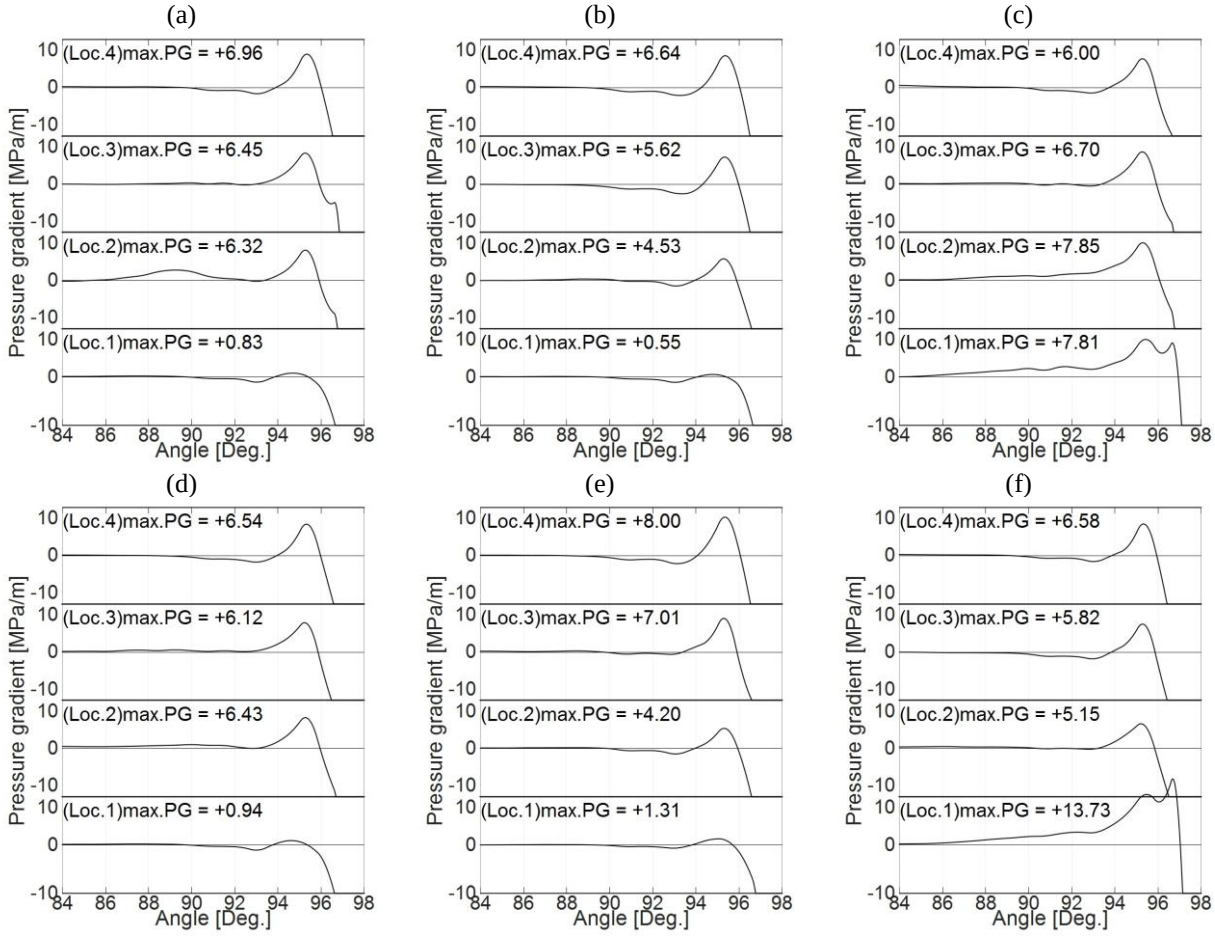

Figure 11: The pressure gradient curves on male rotor surfaces of CFD models named (a) M2, (b) F2, (c) M1F1, (d) M2F2, (e) M3F3, and (f) M1F3.

4. CONCLUSIONS

The ideal CFD model of an oil-injected screw compressor was applied to the study of the rotor lubrication. In the dynamic grid model, the clearance distribution between rotors in the actual contact area was designed by the minimum film thickness, and was 1 μm. The value of this clearance would be affected by the relative speed between rotors, material properties of oil and rotors, curvatures of surfaces, and the condition of load.

The surface oil moved toward the rotor tip and left the rotor surface as the rotor rotation. Although the rotational speed of the male rotor is faster than the one of the female rotor, the average volume fraction of oil on the male rotor surface decreased a little slower than the one on the female rotor surface. The wavy distribution appeared on the part of profile of large radius gradient. The distribution curves on the short side of the tooth profile decreased faster than the one on the long side of the tooth profile. When rotors have rotated one turn, the values of distribution curves on tooth flanks were higher than the ones on roots and tips of rotors.

The axial distribution curves of the volume fraction of oil on rotor surfaces were shown in this study. The pressure gradient on the rotor surface was used to see if the hydrodynamic pressure appeared. In order to achieve a good rotor lubrication, the proper quantity of oil should be maintained on the local surfaces which were going to contact with each other. The pressure gradient and the oil distribution on rotor surfaces would be design objectives of the oil injection, and could be effectively obtained by CFD.

In the future studies of rotor lubrication in the oil-injected screw compressor, the central oil film thickness could be considered in the actual contact area of rotors. The grid model should be improved to obtain a fine spatial resolution in the actual contact area to present the pressure variation of EHD, and to be applied to address the sensitivity of the clearance distribution to the rotor lubrication.

REFERENCES

Basha, N., Rane, S., & Kovacevic, A. (2018). Multiphase Flow Analysis in an Oil-injected Twin Screw Compressor. *Proceedings of the 3rd World Congress on Momentum, Heat and Mass Transfer. doi: 10.11159/icmfht18.132*.

Chevalier, F., Lubrecht, A. A., Cann, P. M. E., Colin, F., & Dalmaz, G. (1998). Film Thickness in Starved EHL Point Contacts. *Journal of Tribology, 120(1)*, 126–133.

Damiens, B., Venner, C. H., Cann, P. M. E., & Lubrecht, A. A. (2004). Starved Lubrication of Elliptical EHD Contacts. J*ournal of Tribology, 126(1)*, 105–111.

Dowson, D. (1969). Elastohydrodynamic Lubrication. In *Interdisciplinary approach to the lubrication of concentrated contacts: proceedings of a NASA-sponsored symposium held July 15-17, 1969, in Troy, New York*. Washington: Scientific and Technical Information Division, National Aeronautics and Space Administration.

Khonsari, M. M., & Booser, E. R. (2008). *Applied Tribology: Bearing Design and Lubrication, Second Edition*. Chichester, England: Wiley.

Kostal, D., Sperka, P., Svoboda, P., Krupka, I., & Hartl, M. (2015). Experimental Observation Of Elastohydrodynamically Lubricated Contacts Replenishment. *MM Science Journal, 2015(03)*, 640–644.

Kostal, D., Sperka, P., Svoboda, P., Krupka, I., & Hartl, M. (2017). Influence of Lubricant Inlet Film Thickness on Elastohydrodynamically Lubricated Contact Starvation. *Journal of Tribology*, *139*(5).

Rane, S., Kovačević, A., & Stošić, N. (2016). CFD Analysis of Oil Flooded Twin Screw Compressors. In *the 23rd International Compressor Engineering Conference at Purdue*.

Zamfirescu, C., Nannan, N., Marin, M. & Infante Ferreira, C.A., (2004). Oil free two phase ammonia (water) compressor. *Final report of NOVEM project BSE-NEO 0268.02.03.03.0002, Delft University of Technology, The Netherlands [report K-336]*.

Zoelen, M. T. V., Venner, C. H., & Lugt, P. M. (2008). Free Surface Thin Layer Flow on Bearing Raceways. *Journal of Tribology, 130*(2).